J Nanopart Res (2019) 21:266
https://doi.org/10.1007/s11051-019-4713-0

RESEARCH PAPER

The comparison of Pr^{3+}:LaF_3 and Pr^{3+}:$LiYF_4$ luminescent nano- and microthermometer performances

M. S. Pudovkin · S. L. Korableva · D. A. Koryakovtseva · E. V. Lukinova · A. V. Lovchev · O. A. Morozov · V. V. Semashko

Received: 2 August 2019 / Accepted: 11 November 2019

Abstract In the present work, we make a comparison of Pr^{3+}:LaF_3 and Pr^{3+}:$LiYF_4$ luminescent nano- and microthermometer performances. We studied Pr^{3+}:LaF_3 nanoparticles, synthesized via co-precipitation method (further Pr_{3+}:LaF_3 (co-precipitation)), Pr^{3+}:LaF_3 nanoparticles, synthesized via hydrothermal method (further Pr^{3+}:LaF_3 (hydrothermal)), and Pr^{3+}:LaF_3 microparticles as well as Pr^{3+}:$LiYF_4$ nanoparticles, synthesized via hydrothermal method (further Pr^{3+}:$LiYF_4$ nanoparticles) and Pr^{3+}:LaF_3 microparticles. According to the X-ray diffraction, Pr^{3+}:LaF_3 (co-precipitation) and Pr^{3+}:LaF_3 (hydrothermal) nanoparticles are hexagonal-structured nanocrystals. Pr^{3+}:$LiYF_4$ nanoparticles are tetragonal-structured nanocrystals. The average diameters of Pr^{3+}:LaF_3 (co-precipitation), Pr^{3+}:LaF_3 (hydrothermal), and Pr^{3+}:$LiYF_4$ nanoparticles are 13.9, 19.4, and 33.3 nm, respectively. The Pr^{3+}:LaF_3 (co-precipitation) and Pr^{3+}:LaF_3 (hydrothermal) nanoparticles demonstrate broadband luminescence caused by crystal lattice defects (luminescence background). This luminescence background notably decreases the temperature sensitivity of these samples. The luminescent background removing procedure significantly complicates the signal processing procedure. Pr^{3+}:LaF_3 microparticles, Pr^{3+}:$LiYF_4$ nanoparticles, and Pr^{3+}:LaF_3 microparticles do not demonstrate this undesirable phenomenon. The absolute temperature sensitivity S_a of Pr^{3+}:$LiYF_4$ nanoparticles, Pr^{3+}:$LiYF_4$ microparticles, and Pr^{3+}:LaF_3 microparticles at 300 K are 0.0117 ± 0.0010, 0.0106 ± 0.0010, and 0.0102 ± 0.0012 K^{-1}, respectively. Although the values of S_a are very close for these samples, the nanosized dimensionality of Pr^{3+}:$LiYF_4$ nanoparticles allows achieving high spatial resolution and expanding the fields of application of Pr^{3+}:$LiYF_4$ nanoparticles.

Keywords Luminescent thermometry · Spectral ratio thermometry · $LiYF_4$ nanoparticles · LaF_3 nanoparticles · Pr^{3+}:$LiYF_4$ · Pr^{3+}: LaF_3

Introduction

Luminescent nanothermometry is a modern highly developing contactless method which allows making temperature mapping with the high spatial and temporal resolution, where the conventional methods are ineffective (Runowski et al. 2019a, b, Liu et al. 2019, Piñol et al. 2019, Brites et al. 2019, Pudovkin et al. 2017). Such specific temperature measurements are required in thermometry of living cells (Yang et al. 2011), temperature mapping of microcircuits (Savchuk et al. 2016), (Liu et al. 2019)(Geitenbeek et al, 2019). The luminescent nanothermometry is based on the temperature-dependent luminescence parameters (intensity, lifetime, band shape, band width, polarization, and spectral position) of special nanosized luminescent materials (Jaque and Vetrone 2012). The known temperature dependence of the luminescent parameter allows performing

M. S. Pudovkin (✉) · S. L. Korableva · D. A. Koryakovtseva · E. V. Lukinova · A. V. Lovchev · O. A. Morozov · V. V. Semashko
Kazan Federal University, Kazan, Tatarstan 420008, Russia
e-mail: jaz7778@list.ru

Published online: 03 December 2019

temperature reading. In turn, nanosized dimensionality of the thermometers and operation in UV, visible of infrared spectral range provide high spatial resolution. One of the most widespread and effective classes of luminescent nanothermometers is based on the temperature dependence of the band shape. In other words, the spectral shape is temperature-dependent. There is a great number of physical mechanisms explaining the temperature dependence of the bandshape luminescent nanothermometer. Briefly, temperature dependence of the bandshape luminescent nanothermometer can be explained by multiphonon relaxation from exited electron levels (Gharouel S et al. 2018), by different processes of energy exchange between optically exited ions (Bednarkiewicz et al. 2015), and by the Boltzmann law (Pudovkin et al. 2017) et al. Specifically, physical background of thermometers based on the Boltzmann law is related to the presence of two thermally coupled electron levels of doping ions which share their electronic populations according to the Boltzmann law. For example, $^3P_1$ and $^3P_0$ levels of Pr^{3+} in LaF_3 (Pudovkin et al. 2017) and YF_3 (Runowski et al. 2019a, b) hosts, $^4I_{15/2}$ and $^4F_{9/2}$ levels of Dy^{3+} in LaF_3 (Bu et al. 2015) and $BaYF_5$ (Liu et al. 2013), and $^2H_{11/2}$ and $^4S_{3/2}$ of Er^{3+} in $NaYF_4$ (Dong et al. 2014) are thermally coupled. This mechanism leads to changing in spectral shape in a specific temperature range. Indeed, according to the Boltzmann law, the population of the higher level increases upon warming which leads to increasing of emission intensity of this level. In this case, the studied temperature-dependent parameter is integrated intensity ratio of emission intensities of these two thermally coupled levels. This ratio defines absolute and relative sensitivities described in many works (Pudovkin et al. 2017; Dong et al. 2014; Bu et al. 2015). If this changing in intensities is fully described by the Boltzmann, the temperature sensitivity depends on energy gap between these two levels only. The energy gap is affected by several factors including host matrix. The temperature sensitivity can be optimized by choosing the doping ion and the host matrix.

However, such parameters as photostability, brightness, and easiness of the luminescence signal procession no less important than the temperature sensitivity. Among luminescent materials, rare earth-doped fluoride bulk and nanomaterials hold special role because of their excellent photostability and chemical stability (Feng et al. 2010; Clement et al. 2015; Jia et al. 2013), long luminescent lifetimes, sharp emission bands (Rahman and Green 2009), low possibility of nonradiative transitions (Li and Lin 2010), and low toxicity (Nizamutdinov et al. 2007; Pudovkin et al. 2018; Semashko et al. 2018; Pudovkin et al. 2016). However, such nanomaterials differ between each other by brightness, peak positions, presence of undesirable luminescence background, etc. Indeed, low brightness leads to low signal-to-noise ratio which is a common source of inaccuracies. The presence of luminescence background is observed in a list of works devoted to optical properties on nanomaterials (Kuznetsov et al. 2018; Zhou et al. 2014). This phenomenon is explained by relaxation processes of the excited crystal lattice defects (Rakhmatullin et al. 2019). These relaxation processes can be temperature-dependent and make positive or negative contributions into temperature sensitivity simultaneously complicating signal processing procedure. The physical mechanism of luminescence background is related to many factors including defects. The description of this mechanism is complex. Indeed, the number of defects and their nature depend on the chemical composition of the materials as well as on the synthesis procedure. For instance, the nature of defects of LaF_3 and DyF_3 nanoparticles is different. Additionally, the number of defects in nanoparticles can be restricted by hydrothermal treatment (Pudovkin et al. 2019a, b), annealing (Kuznetsov et al. 2018), or simultaneous hydrothermal and microwave treatment (Vanetsev et al. 2017). Hence, the luminescence background should be removed during the signal processing procedure or prevented by the synthesis procedure. The comparison of luminescent thermometer performances can help in the choice of proper and most effective material for a specific task. In this work, LaF_3 and $LiYF_4$ as host matrices were chosen. These matrices are considered very promising for many brunches of science (Kim et al. 2015; Wang et al. 2010; Yu et al. 2014; Khiari et al. 2008; Becerro et al. 2015). Particularly, rare earth-doped LaF_3 nanomaterials are relatively well-studied. However, such features as luminescent background and easiness of signal processing procedures are not discussed enough. In contrast, $LiYF_4$ nanomaterials are not such well-studied. Moreover, according to (Ye et al. 2015; Mahalingam et al. 2009), $LiYF_4$ host generates additional emission lines which can contribute to the temperature sensitivity of $LiYF_4$-based thermometers. The Pr^{3+}-based thermometers demonstrates good thermometer performances (Gharouel et al. 2019, Pudovkin and Rakhmatullin 2020).

Here we make a comparison of Pr^{3+}-doped LaF_3 and $LiYF_4$ luminescent nano- and microthermometer performances. We studied Pr^{3+}:LaF_3 nanoparticles,

synthesized via co-precipitation method (further Pr^{3+}:LaF_3 (co-precipitation)), Pr^{3+}:LaF_3 nanoparticles, synthesized via hydrothermal method (further Pr^{3+}:LaF_3 (hydrothermal)), and Pr_{3+}:LaF_3 microparticles, as well as Pr^{3+}:$LiYF_4$ nanoparticles, synthesized via hydrothermal method (further Pr^{3+}:$LiYF_4$ nanoparticles), and Pr^{3+}:LaF_3 microparticles. (Note that Pr^{3+}:$LiYF_4$ nanoparticles cannot be synthesized via co-precipitation method.) LaF_3 and $LiYF_4$ hosts differ between each other by many factors including symmetry, phonon energy, number of defects, etc. We analyze the possibility of using Pr^{3+} doped LaF_3 and $NaYF_4$ nano- and microparticles in luminescent thermometry by several criteria such as temperature sensitivity, presence of undesirable luminescence background, and easiness of signal processing.

The aim of the work is to choose the best luminescent thermometer among the studied ones by such criteria as absolute temperature sensitivity, easiness of signal processing, size of the thermometers, and presence of luminescent background.

Materials and methods

Materials

All the chemicals used are of analytical grade. The $Ln(NO_3)_3 \cdot 6H_2O$ (Ln = Y, and Pr), oleic acid, ammonium fluoride, lithium hydroxide, ethanol, nitric acid, and cyclohexane were purchased from Sigma–Aldrich. All the chemicals were used without further purification.

Synthesis of the sample

The doping concentrations of Pr^{3+} were set as 1.0 mol% for all the samples.

The Pr^{3+}:$LiYF_4$ nanoparticles were prepared by the modified solvothermal method (Fedorov et al. 2011). First, 2.898 g $LiOH{\cdot}H_2O$ and 30 mL deionized water, 54 mL oleic acid, and 90 ml ethanol were mixed by vigorous stirring at 55 °C for 30–40 min until a transparent solution appeared. Second, 12 ml of an aqueous solution containing 1.084 g of $Y(NO_3)_3{\cdot}5H_2O$ and 0.013 g of $Pr(NO_3)_3{\cdot}6H_2O$ was added to the mixture. Third, 0.444 g of NH4F in 12 ml of deionized water was added drop by drop to the homogeneous solution and vigorously was stirred for 5 minutes. Without any adjustment of the pH of the resulting stock, solution was 7.0. Finally, this mother solution was transferred into Teflon-lined autoclave and heated at 130 °C for 5 h. The precipitated nanoparticles were collected by centrifugation, washed using water–ethanol mixture and ethanol several times, and dried at the air at 60 °C for 24 h. The dried powder samples were pressed into disks of 2 nm thick and 5 nm in diameter for the spectral measurements.

The Pr^{3+}:LaF_3 (C_{Pr} = 1%) nanoparticles were synthesized via co-precipitation from aqueous solution (Semashko et al. 2018). In order to synthesize Pr^{3+}:LaF_3 (C_{Pr} = 1%) nanoparticles, 0.041 g of Pr_2O_3 and 4.007 g La_2O_3 were added to 85 mL of 10% nitric acid in a glass beaker. The mixture was heated to 50 °C and stirred for 45 min until a transparent solution appeared. Then the solution was filtered, poured in a polypropylene glass, and put on the magnetic mixer (400 rpm). The solution of NaF was prepared by adding of 3.8 g of NaF into 500 mL of deionized water. After filtration of the NaF, solution was swiftly poured. Then the pH was adjusted to 4 by adding 25% solution of ammonium hydrate. Then the mixture was stirring for 30 minutes (400 rpm) and then the nanoparticles were washed by centrifugation (Janetski K24; 12000 rpm) using deionized water for several times. The nanoparticles were dried at the air at 60 °C for 24 h.

The Pr^{3+}:LaF_3 and the Pr^{3+}:$LiYF_4$ crystals with doping concentration of 1 at.% were grown from a mixture of commercial high purity powders (99.999%) in a carbon crucible in Ar atmosphere with Teflon burning. In the case of Pr^{3+}:LaF_3, the crucible was heated by inductive heating above the melting point of LaF_3 to about 1530 °C and cooled down for 96 h to room temperature. The Pr^{3+}:$LiYF_4$ crystal was grown by the Bridgman technique from the melt containing 52% LiF and 48% YF_3 at the rate of 1.3 mm/hr (Shavelev et al. 2014; Lyapin et al. 2016). The crystals were milled in an automatic mill (Minpribor-0309). The obtained crystalline particles were sieved with the 0.45 mm pore size sieve in order to remove big (> 0.45 mm) particles.

Characterization of the samples and thermometric experiments

The structure of the material was characterized by X-ray diffraction method (XRD) with Shimadzu XRD-7000S X-ray diffractometer. Transmission electron microscopy (TEM) experiments were carried out in a transmission electron microscope Hitachi HT7700 Exalens. Sample

preparation: the suspension (10 microliters) was placed on a formvar/carbon lacey 3 mm copper grid; drying was performed at room temperature. After drying, the grid was placed in a transmission electron microscope using a special holder for microanalysis. The analysis was held at an accelerating voltage of 100 kV in TEM mode. The luminescence spectra were recorded using CCD spectrometer (StellarNet), which detects the emission in 200–1100 nm spectral range with a spectral resolution of 0.5 nm. The optical parametric oscillator laser system (420–1200 nm) from JV LOTIS TII was used for excitation of the luminescence of the samples. The pulse width and the pulse repetition rate were 10 ns and 10 Hz, respectively. The spectral width of laser radiation was less than 0.15 nm. The experiments were carried out in 80–320 K temperature range. The temperature control was carried out via thermostatic cooler "CRYO industries" having LakeShore Model 325 temperature controller. The liquid nitrogen was used as a cooling agent.

Results and discussion

Characterization of the samples

According to the TEM data, Pr^{3+}:$LiYF_4$ nanoparticles have an average diameter of 38 ± 2 nm. It can be observed that the shape of the nanoparticles varies from almost spherical to rhombic (Fig. 1a). Herewith, the shape becomes more rhomb-like with increasing of the size of the nanoparticles. The same phenomenon was of observed in [3]. High-resolution TEM (HRTEM) image reveals the crystalline nature of the Pr^{3+}:$LiYF_4$ nanoparticles (Fig 1b). The HRTEM image also shows lattice fringes with observed d-spacing of ~0.46 nm corresponding to lattice spacing in the (011) planes of tetragonal phase $LiYF_4$.

TEM and HRTEM images of the Pr^{3+}:LaF_3 (co-precipitation) nanoparticles are represented in Fig. 2a and b, respectively. The nanoparticles have relatively irregular shape without the preferred direction of growth as it is commonly expected for co-precipitation method (Ma et al. 2007; Pudovkin et al. 2018). The average diameter of the nanoparticles is equal to 13.9 nm. The TEM and HDTEM images of the Pr^{3+}:LaF_3 (hydrothermal) nanoparticles are represented in Fig. 2c and d, respectively. The shape of the nanoparticles became significantly more regular. The average diameter of the nanoparticles is 19.4 nm. In some nanoparticles, the 3–8 nm clusters can be clearly observed. According to the work (Alakshin et al. 2012), these clusters may contain water which is typical for this kind of hydrothermal synthesis (Wang and Li 2003). The HRTEM image (Fig. 2b, d) also shows lattice fringes with observed spacing of around 0.35 nm corresponding to lattice spacing in the (111) planes of hexagonal phase of LaF_3 for both kinds of Pr^{3+}:LaF_3 nanoparticles. The increase in size of the nanoparticles after hydrothermal treatment can be related to the recrystallization–dissolution process and the Ostwald ripening (Ma et al. 2007).

The XRD patterns of Pr^{3+}:LaF_3 and Pr^{3+}:$LiYF_4$ nanoparticles are represented in Fig. 3. According to the XRD data, the Pr^{3+}:LaF_3 nanoparticles are hexagonal-structured nanocrystals that corresponds to the structure of matrices of LaF_3 and PrF_3. In case of Pr^{3+}:$LiYF_4$ nanoparticles, all the diffraction peaks can be well indexed in accordance with tetragonal $LiYF_4$ crystal (JCPDS file No. 81-2254), indicating the formation of tetragonal phase of the $LiYF_4$ nanoparticles. Sharp peaks and lack of peaks from impurities are observed, suggesting the high purity of these samples. The lattice parameters a and c of both types of the Pr^{3+}:LaF_3 nanoparticles and the Pr^{3+}:$LiYF_4$ nanoparticles are listed in Table 1. The slight difference in obtained lattice parameters and values of the lattice parameters from JCPDS can be related to the presence of doping ion Pr^{3+}. Indeed, the ionic radius of Pr^{3+} (1.05 Å) is smaller than that of La^{3+} (1.13 Å) due to the lanthanide contraction, so the cell volume of Pr^{3+}:LaF_3 reduces with more Pr^{3+} replacing La^{3+}, which results in changing of the lattice parameters. The ionic radii of Y^{3+} and Li^{+} are equal to 2.4 and 1.82 Å, respectively; hence the cell volume changing may also take place. The increased role of surface as well as presence of defects can also affect the lattice parameters (Guozhong 2004, Rao et al. 2006).

The information concerning the sizes of coherent scattering domains can be extracted from the XRD patters. The comparison of sizes of the coherent scattering domains at different crystallographic orientations (determined by the Miller indices (hkl)) allows estimating the degree of the shape isotropy. In order to estimate sizes of coherent scattering domains of the nanoparticles, the Debye–Scherrer method is used (Scherrer 1918):

$$D = \frac{K\lambda}{\beta_D Cos\theta} \quad (1)$$

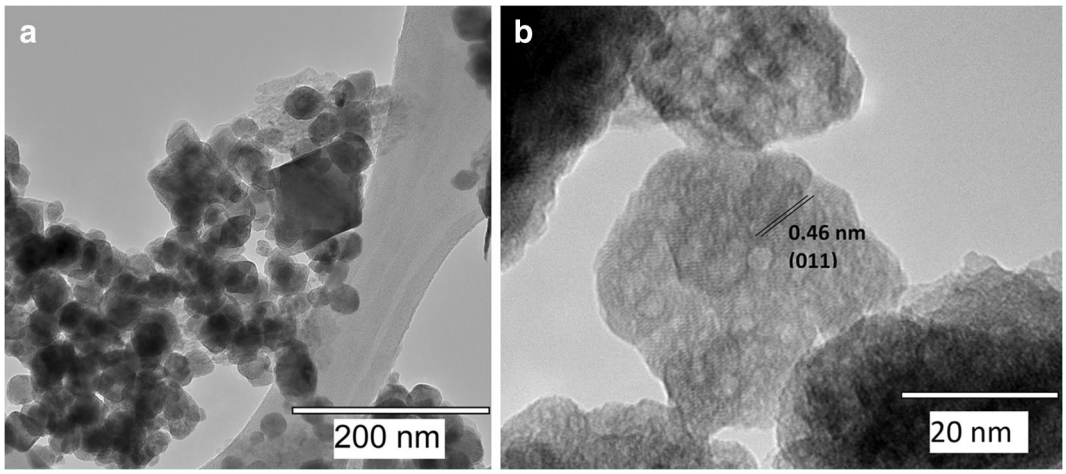

Fig. 1 **a** TEM image of the Pr^{3+}:$LiYF_4$ nanoparticles. **b** High-resolution TEM image of the Pr^{3+}:$LiYF_4$ nanoparticles

where D is a size of the coherent scattering domain of a nanoparticle, K is a shape factor (we used K = 0.9), λ is the X-ray wavelength (0.15418 nm), β_D is the line broadening at half the maximum intensity (FWHM) in radians, and θ is the Bragg's angle. The diffraction peaks having the highest values of the signal-to-noise ratio are chosen. The calculation of values of D at different crystallography orientations (D_{hkl}) allows estimating shape isotropy and revealing the preferred growth direction of nanocrystals (Pudovkin et al. 2019a). Particularly, in work (Pudovkin et al. 2019a) anisotropic in shape, plate-like Pr^{3+}:LaF_3

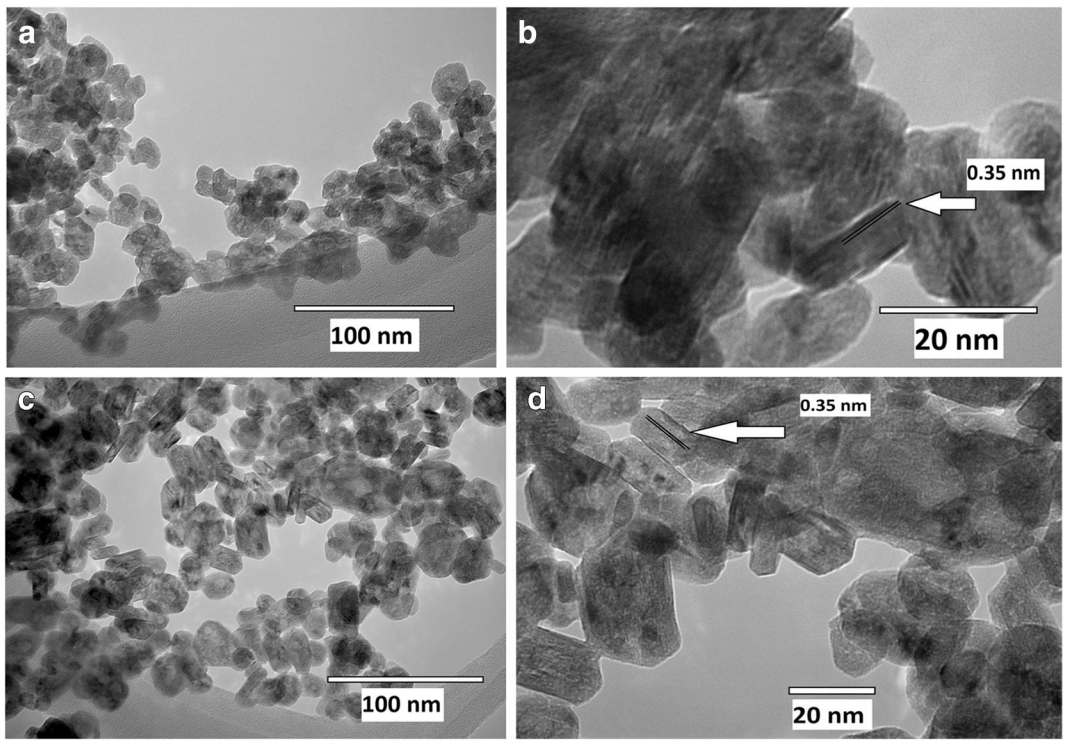

Fig. 2 **a** TEM image of the Pr^{3+}:LaF_3 nanoparticles synthesized via co-precipitation method. **b** HRTEM image of the Pr^{3+}:LaF_3 nanoparticles synthesized via co-precipitation method. **c** TEM image of the Pr^{3+}:LaF_3 nanoparticles synthesized via hydrothermal method. **d** HRTEM image of the Pr^{3+}:LaF_3 nanoparticles synthesized via hydrothermal method

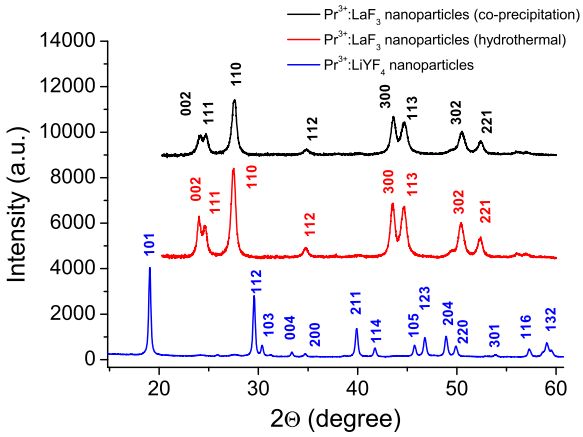

Fig. 3 X-ray diffraction patterns of the Pr^{3+}:LaF_3 nanoparticles, synthesized via co-precipitation method, Pr^{3+}:LaF_3 nanoparticles, synthesized via hydrothermal method, and Pr^{3+}:$LiYF_4$ nanoparticles

nanoparticles demonstrate notable dependence of all D_{hkl} values on crystallography orientation for several directions (hkl). The standard deviation for the list of D_{hkl} values in (Pudovkin et al. 2019a) is 5.1 nm which characterize notable difference of D_{hkl} between each other. The sphere-like Pr^{3+}:LaF_3 nanoparticles do not demonstrate such tendency (Pudovkin et al. 2019a).

Here we also estimate the values of D_{hkl} at different crystallography orientations in order to additionally characterize the morphology of the studied nanoparticles. The sizes of D_{hkl} in different crystallography orientations (hkl) for Pr^{3+}:LaF_3 (co-precipitation), Pr^{3+}:LaF_3 (hydrothermal), and Pr^{3+}:$LiYF_4$ nanoparticles are listed in Tables 2 and 3, respectively.

The sizes of coherent scattering domains at different crystallographic directions (hkl) D_{hkl} of Pr^{3+}:LaF_3 (co-precipitation) nanoparticles slightly differ between each other. However, it seems that there is no any preferred growth direction of Pr^{3+}:LaF_3 (co-precipitation) nanoparticles. The difference of D_{hkl} for Pr^{3+}:LaF_3 (hydrothermal) nanoparticles is more pronounced. The difference in the values of the standard deviation (SD) for Pr^{3+}:LaF_3 (co-precipitation) (1.1 nm) and Pr^{3+}:LaF_3 (hydrothermal) (2.7 nm) confirms this fact. Indeed, according to the TEM data, some Pr^{3+}:LaF_3 (hydrothermal) nanoparticles have slightly prolate form. Probably, the notable difference in D_{002} (21.1 nm), D_{300} (16.5 nm), and D_{113} (13.6 nm) additionally confirms this slight shape anisotropy. The TEM data do not reveal such a tendency for Pr^{3+}:LaF_3 (co-precipitation) nanoparticles.

Table 1 Lattice parameters of Pr^{3+}:LaF_3 and Pr^{3+}:$LiYF_4$ nanoparticles

Sample/parameter	a (nm)	c (nm)
Pr^{3+}:LaF_3 nanoparticles (co-precipitation)	0.7197	0,7375
Pr^{3+}:LaF_3 nanoparticles (hydrothermal)	0.7201	0.7432
Pr^{3+}:$LiYF_4$ nanoparticles	0.5161	1.0805
LaF_3 (JCPDS–32–0483)	0.7186	0.7352
$LiYF_4$ (JCPDS 81-2254)	0.5171	1.0748

The values of D_{hkl} for Pr^{3+}:$LiYF_4$ nanoparticles do not demonstrate a significant difference (SD = 1.8 nm). The TEM data also confirm this tendency. Although there are some rhombic nanoparticles, their amount is small in comparison with spherical-like nanoparticles. It should be noted that the physical size and the coherent scattering domains are not the same. However, close amounts of average D_{hkl} and physical sizes (D_{TEM}) for all the nanoparticles indicate that each nanoparticle is the whole unified crystalline formation instead of smaller particle or domain agglomerates, which is good for luminescence purposes.

Performances of the luminescent thermometers based on Pr^{3+}:$LiYF_4$ nanoparticles and Pr^{3+}:$LiYF_4$ microparticles

The normalized luminescent spectra of Pr^{3+}:$LiYF_4$ nanoparticles and Pr^{3+}:$LiYF_4$ microparticles obtained at 300 K are shown in Fig.4. It can be seen that the spectra are identical. It seems that the size effect caused mostly by the increased role of the surface do not influence the luminescence properties. Indeed, according to (Vanetsev et al. 2017) for the nanoparticles having average size more than 10–15 nm, the role of the surface is not significant. Thus, the surface Pr^{3+} ions located into reduced symmetry crystal field do not affect much the luminescence properties of the nanoparticles. The luminescent spectra have the emissions bands which are interpreted as the result of the transition from the ^3P_j (j = 0, 1) excited states to $^3H_4$ and $^3H_5$ states of Pr^{3+}ions (Müller et al. 2012).

The normalized luminescent spectra of Pr^{3+}:$LiYF_4$ nanoparticles and Pr^{3+}:$LiYF_4$ microparticles as a function of temperature are shown in Fig. 5a and b, respectively. It is clearly seen that the emission from $^3P_1$ state is not observed in 80–120 K temperature range. Then, the $^3P_1$ emission increases with the increase of the temperature in 140–320 K temperature range. This

Table 2 The sizes of coherent scattering domains D_{hkl} of the Pr^{3+}:LaF_3 nanoparticles in different crystallography orientations (hkl), the values of standard deviation (SD) (nm), and the physical size of the nanoparticles D_{TEM} (nm) obtained from TEM data

Sample/(D_{hkl} (nm)	D_{002}	D_{110}	D_{111}	D_{300}	D_{113}	SD	Average D_{hkl}	D_{TEM} (nm)
Pr^{3+}:LaF_3 nanoparticles (co-precipitation)	14.6	17.4	15.2	15.9	14.5	1.1	15.3	13.9
Pr^{3+}:LaF_3 nanoparticles (hydrothermal)	21.1	17.3	16.4	16.2	13.6	2.7	17.0	19.4

phenomenon can be attributed to the fact that $^3P_1$ and $^3P_0$ states share their electronic populations according to the Boltzmann process (Runowski et al. 2019a, b). Indeed, according to the experimental data, the thermalization of $^3P_1$ state begins at around ~140 K and operates more and more efficiently upon warming. For such luminescent thermometers, the luminescence intensity ratio (LIR) of two thermally coupled emission peaks is taken as a temperature-dependent parameter (Jaque and Vetrone 2012; Brites et al. 2016). If in the studied system only Boltzmann law is responsible for temperature sensitivity of the LIR can be described as (Brites et al. 2016):

$$LIR = Bexp\left(\frac{\Delta E}{k_B T}\right) + C \tag{2}$$

where B and C are constants, ΔE is activation energy (here the energy difference between the $^3P_1$ and $^3P_0$ states), k_B is the Boltzmann constant, and T is the absolute temperature. Two distinct emission bands in the 510–536 and 536–570 nm spectral ranges, corresponding to the $^3P_1 \rightarrow {}^3H_5$ and $^3P_0 \rightarrow {}^3H_5$ transitions, respectively, were chosen for calculations of the LIR. The LIR plots for Pr^{3+}:$LiYF_4$ nanoparticles and Pr^{3+}:$LiYF_4$ microparticles are shown in Fig. 6a. The LIR curves for both Pr^{3+}:$LiYF_4$ nanoparticles and Pr^{3+}:$LiYF_4$ microparticles can be described by Eqs. 3 and 4, respectively:

$$LIR\ (\text{nanoparticles}) = (15.3 \pm 0.5)exp\left(\frac{691 \pm 6}{T}\right) + 0.24 \tag{3}$$

$$LIR\ (\text{microparticles}) = (14.0 \pm 03)exp\left(\frac{699 \pm 7}{T}\right) + 0.13 \tag{4}$$

The values of ΔE of Pr^{3+}:$LiYF_4$ nanoparticles and Pr^{3+}:$LiYF_4$ microparticles are 480 ± 4 and 486 ± 4 cm^{-1}, respectively. Both LIR functions are almost identical within the accuracy of the calculations. Absolute (S_a) and relative (S_r) temperature sensitivities can be written as (Jaque and Vetrone 2012, Brites et al. 2016):

$$S_a = \frac{1}{R}\frac{d(LIR)}{dT} = \frac{\Delta E}{k_B T^2} \tag{5}$$

$$S_r = \frac{d(LIR)}{dT} = R\left(\frac{\Delta E}{k_B T^2}\right) \tag{6}$$

S_a and S_r plots of both Pr^{3+}:$LiYF_4$ nanoparticles and Pr^{3+}:$LiYF_4$ microparticles are represented in Fig. 6b. The S_a values of Pr^{3+}:$LiYF_4$ nanoparticles and Pr^{3+}:$LiYF_4$ microparticles at 300 K are equal to 0.0106 ± 0.001 K^{-1} and 0.0117 ± 0.001 K^{-1}.

Nanothermometers' performances of Pr^{3+}:LaF_3 (co-precipitation), Pr^{3+}:LaF_3 (hydrothermal) nanoparticles, and Pr^{3+}:LaF_3 microparticle

The normalized luminescent spectra of Pr^{3+}:LaF_3 (co-precipitation) nanoparticles, Pr^{3+}:LaF_3 (hydrothermal) nanoparticles, and Pr^{3+}:LaF_3 microparticles obtained at 300 K are shown in Fig. 7. The luminescent spectra have the emission bands which are interpreted as the result of

Table 3 The values of coherent scattering domains D_{hkl} of the Pr^{3+}:$LiYF_4$ nanoparticles in different crystallography orientations (hkl), the values of standard deviation (SD) (nm), and the physical size of the nanoparticles D_{TEM} (nm) obtained from TEM data

Sample/(D_{hkl} (nm)	D_{110}	D_{112}	D_{221}	D_{114}	D_{105}	D_{123}	D_{204}	D_{220}	SD	Average D_{hkl}	D_{TEM} (nm)
Pr^{3+}:$LiYF_4$ nanoparticles	34.2	33.3	30.7	33.7	32.0	30.2	29.9	29.4	1.8	31.6	33.3

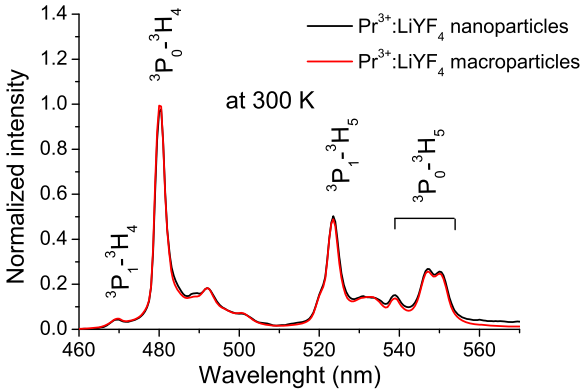

Fig. 4 Normalized luminescence spectra of the Pr^{3+}:$LiYF_4$ nanoparticles and the Pr^{3+}:$LiYF_4$ microparticles at 300 K (normalized at 480 nm, λ_{ex} = 444 nm). Negligible luminescent background takes place in case of Pr^{3+}:$LiYF_4$ nanoparticles

the transition from the ^3P_j (j = 0, 1) excited states to $^3H_4$, $^3H_5$, $^3H_6$, $^3F_2$, and $^3F_4$ states of Pr^{3+}ions (Müller et al. 2012). Any unidentified emission peaks are not observed. The peak positions of Pr^{3+}:LaF_3 nanoparticles and Pr^{3+}:LaF_3 microparticles do not differ between each other as it is observed for Pr^{3+}:$LiYF_4$ samples discussed above. However, clear broad luminescence background in 500–600 nm spectral range is observed for both Pr^{3+}:LaF_3 (co-precipitation) and Pr^{3+}:LaF_3 (hydrothermal) nanoparticles. However, the luminescent background is more pronounced in the case of Pr^{3+}:LaF_3 (co-precipitation) nanoparticles. This phenomenon can be explained by the relaxation processes of the excited crystal lattice defects of the investigated particles (Kuznetsov et al. 2018; Rakhmatullin et al. 2019). Indeed, the fluoride nanoparticles synthesized via co-precipitation method contain a larger number of defects in comparison with nanoparticles subjected to hydrothermal treatment (Pudovkin et al. 2019a; Vanetsev et al. 2017; Fedorov et al. 2011). Additionally, the average diameter of the Pr^{3+}:LaF_3 (hydrothermal) nanoparticles is bigger than the average diameter of Pr^{3+}:LaF_3 (co-precipitation) nanoparticles. It means that the role of surface defects is reduced in the case of Pr^{3+}:LaF_3 (hydrothermal) nanoparticles in comparison with Pr^{3+}:LaF_3 (co-precipitation) nanoparticles. The luminescence spectrum of Pr^{3+}:LaF_3 microparticles does not demonstrate the luminescent background. Indeed, the bulk crystals contain significantly less number of defects (Vanetsev et al. 2017). The luminescent background can affect the temperature sensitivity of the luminescent materials.

It should be noted that the background luminescence phenomenon for optical inorganic materials is considered undesirable. According to the literature data, it can be related to the presence of defects, impurities, as well as to the optical properties of the host. Specifically, in (Fu et al. 2015) for the Eu^{3+},Tb^{3+}:$Ca_5(PO_3)_3F$ microparticles synthesized via citrate-assisted method, the broad blue emission peak was observed under 299 nm laser excitation. The authors suggested that this blue light emission of the host matrix might originate from the CO_2 radical-related defect produced by Cit^{3-} groups. In (Pan et al. 2008), terbium-activated lithium–lanthanum–aluminosilicate oxyfluoride scintillating glass (LLASOF) also demonstrates the luminescence background. The authors suggested that it can be related to the presence of nonbridging oxygen defects in the glass. These nonbridging oxygen defects in LCASOF are a strong source of charge traps and may be responsible for

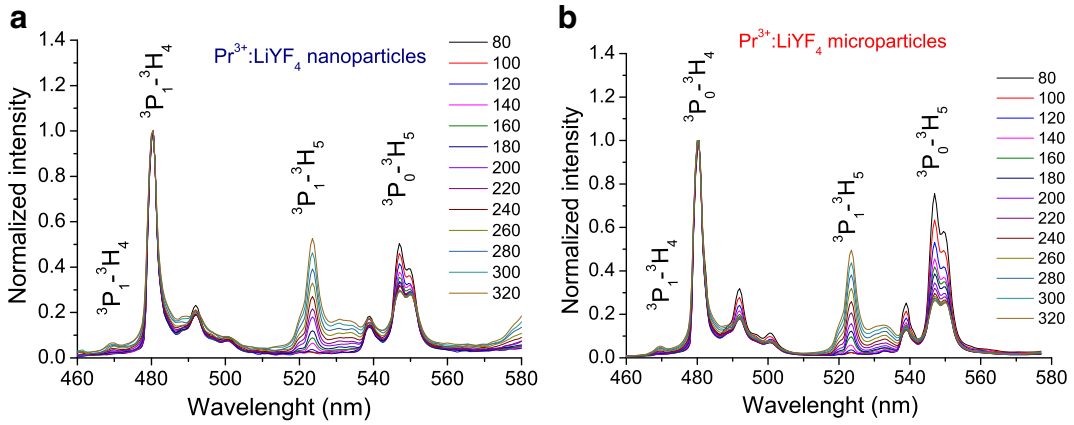

Fig. 5 Normalized luminescence spectra of the Pr^{3+}:$LiYF_4$ nanoparticles (a) and the Pr^{3+}:$LiYF_4$ microparticles (b) as a function of temperature (normalized at 480 nm, λ_{ex} = 444 nm)

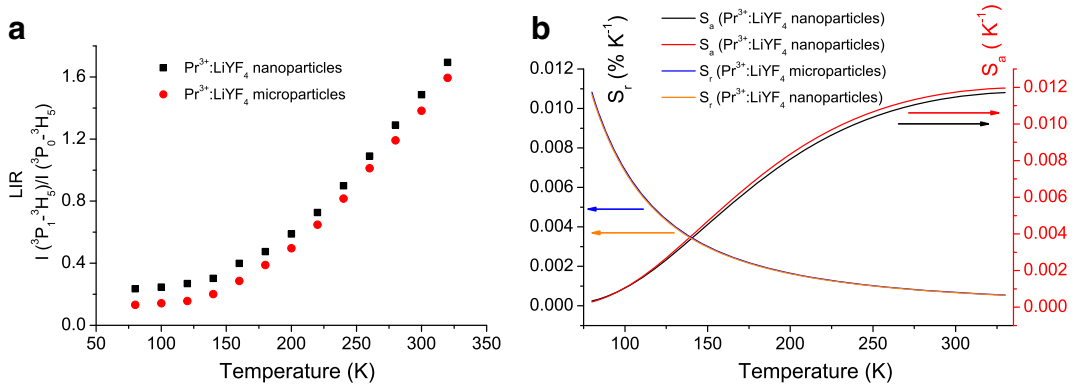

Fig. 6 **a** Integrated intensity ratio of Pr^{3+}:$LiYF_4$ nanoparticles and the Pr^{3+}:$LiYF_4$ microparticles as function of temperature. **b** Absolute and relative temperature sensitivity curves of Pr^{3+}:$LiYF_4$ nanoparticles and the Pr^{3+}:$LiYF_4$ microparticles

the reduced luminescence of doping ions. In (Rakhmatullin et al. 2019), it was made a suggestion that the origin of the background for Pr^{3+}:LaF_3 nanoparticles depends on the synthesis procedure. In this work, it was prepared with two Pr^{3+}:LaF_3 samples. The first sample was Pr^{3+}:LaF_3 nanoparticles synthesized via co-precipitation method and then dried in air and annealed in a vacuum chamber at 300 °C. The second sample was not annealed. The annealed sample became brown which can be related to oxyfluoride formation. This sample demonstrates intense luminescence background which is attributed to the excitation energy transfer from Pr^{3+} to oxygen. The sample which was not annealed with the luminescence background is less intense and can be related to the relaxation processes of the excited crystal lattice defects (here fluoride vacancies). Davies et al. 2017 studied optical properties of a new Eu^{3+}-based metallasilsesquioxane species. They also observe a baseline which is attributed to the presence of hydrocarbon defects, which becomes enhanced by thermal treatment.

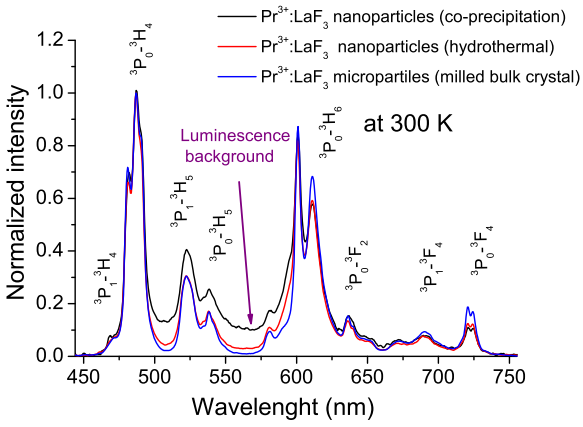

Fig. 7 Normalized luminescence spectra of the Pr^{3+}:LaF_3 samples at 300 K (normalized at 480 nm, λ_{ex} = 444 nm). Negligible luminescent background takes place in case of Pr^{3+}:LaF_3 nanoparticles synthesized via hydrothermal method, the notable luminescent background takes place in case of Pr^{3+}:LaF_3 nanoparticles synthesized via co-precipitation method

The luminescent spectra of Pr^{3+}:LaF_3 (co-precipitation) nanoparticles, Pr^{3+}:LaF_3 (hydrothermal) nanoparticles, and Pr^{3+}:LaF_3 microparticle as a function of temperature are shown in Fig. 8a, b, and c, respectively. As it is clearly seen, the emission from $^3P_1$ state is not observed in 80–120 K temperature range. Then, the $^3P_1$ emission increases with the increase of temperature in 140–320 K temperature range. This phenomenon can also be attributed to the fact that $^3P_1$ and $^3P_0$ states share their electronic populations according to the Boltzmann process. These processes look similar for all the Pr^{3+}:LaF_3 samples. However, in the case of samples Pr^{3+}:LaF_3 (co-precipitation), Pr^{3+}:LaF_3 (hydrothermal) luminescence background becomes more pronounced in the 280–320 K temperature range.

The LIR plots of Pr^{3+}:LaF_3 (co-precipitation), Pr^{3+}:LaF_3 (hydrothermal) nanoparticles, and Pr^{3+}:LaF_3 microparticle are shown in Fig. 9a. The LIR plots differ between each other notably. Specifically, the LIR plot of the Pr^{3+}:LaF_3 (hydrothermal) nanoparticles seems to be less temperature-dependent in comparison with the LIR plot of Pr^{3+}:LaF_3 microparticles. Moreover, the LIR plot of Pr^{3+}:LaF_3 (co-precipitation) nanoparticles does not even demonstrate temperature dependence into 240–320 K temperature range. It seems that the luminescence background decreases the degree of temperature dependency of the LIR plots of both Pr^{3+}:LaF_3 (co-precipitation) and Pr^{3+}:LaF_3 (hydrothermal) nanoparticles. It can be concluded that the resulting LIR curve of both Pr^{3+}:LaF_3 (co-

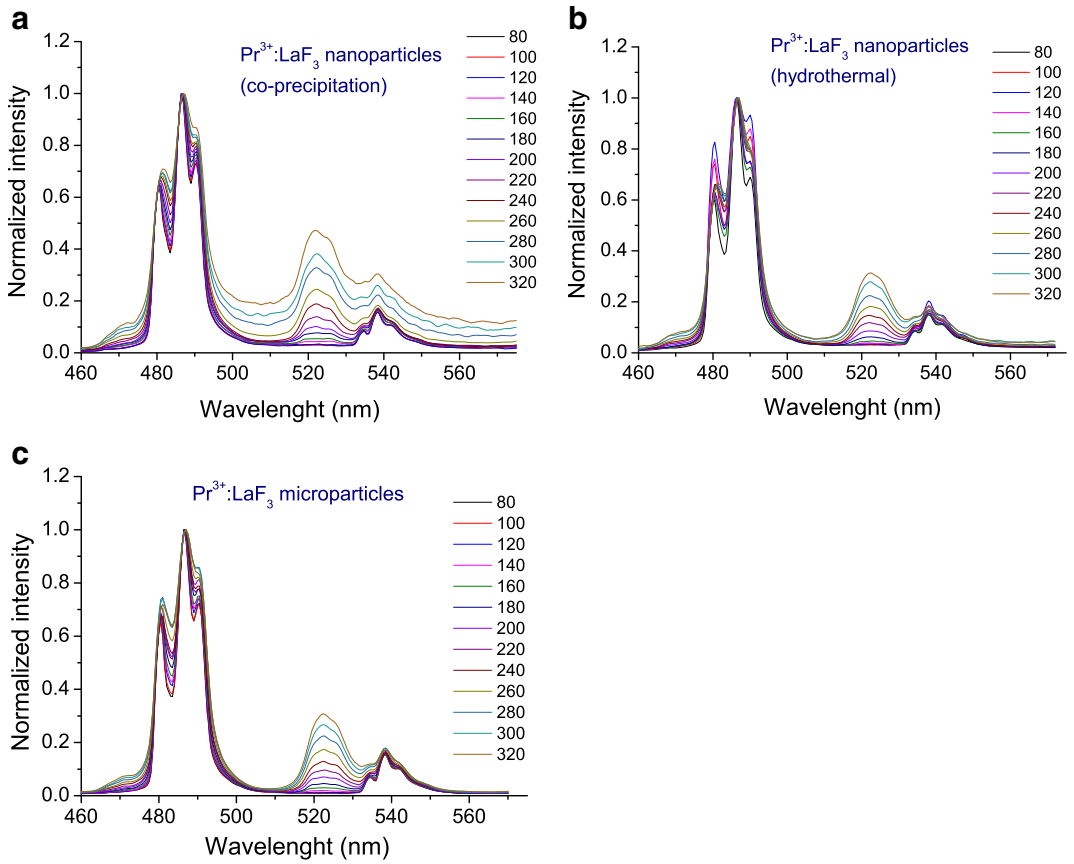

Fig. 8 a, b, c Normalized luminescence spectra of the Pr^{3+}:LaF_3 nanoparticles synthesized via co-precipitation method (a), Pr^{3+}:LaF_3 nanoparticles synthesized via hydrothermal method (b), and the Pr^{3+}:LaF_3 microparticles (c) as a function of temperature (normalized at 486 nm, λ_{ex} = 444 nm)

precipitation) and Pr^{3+}:LaF_3 (hydrothermal) nanoparticles is a function of the Boltzmann process and a set of the physical processes triggering the luminescence background. The theoretical description of these physical processes is nontrivial. Hence, in order to obtain optimized thermometer performance, the luminescence background should be minimized or removed. However, the removing procedure gives rise to uncontrolled mistakes as well as complicates signal processing procedures. Hence, it seems that the best decision is to construct luminescence thermometer which performs without the luminescence background.

Indeed, after luminescence background removing of the Pr^{3+}:LaF_3 (hydrothermal) nanoparticles, the LIR curves of Pr^{3+}:LaF_3 (hydrothermal) nanoparticles and Pr^{3+}:LaF_3 microparticles became almost identical (Fig. 9b).

It's fair that in case of Pr^{3+}:LaF_3 samples, the Boltzmann law can be applied for Pr^{3+}:LaF_3 microparticles. The LIR plot of the Pr^{3+}:LaF_3 microparticles is described by Eq. 7:

$$LIR\left(\mathrm{Pr^{3+}:LaF_3\ microparticles}\right) = (14.3 \pm 0.1)exp\left(\frac{729 \pm 11}{T}\right) + 0.11 \quad (7)$$

The value of ΔE of Pr^{3+}:LaF_3 microparticles is 507 ± 6 cm^{-1}. According to the theoretical calculation, the values of ΔE for Pr^{3+}:LaF_3 and Pr^{3+}:$LiYF_4$ are equal to 587 cm^{-1} (Carnall et al. 1969) and 556 cm^{-1} (Esterowitz et al. 1979), respectively. The S_a and S_r curves are represented in Fig. 9c. The values of S_a and ΔE are listed in Table 4.

It can be seen that the values of S_a and ΔE do not differ between each other significantly. Indeed, the S_a is mostly determined by ΔE in the model based on Boltzmann law. Hence a slight difference in ΔE gives rise to a slight difference in S_a. However, the difference between theoretical ΔE and ΔE determined in the

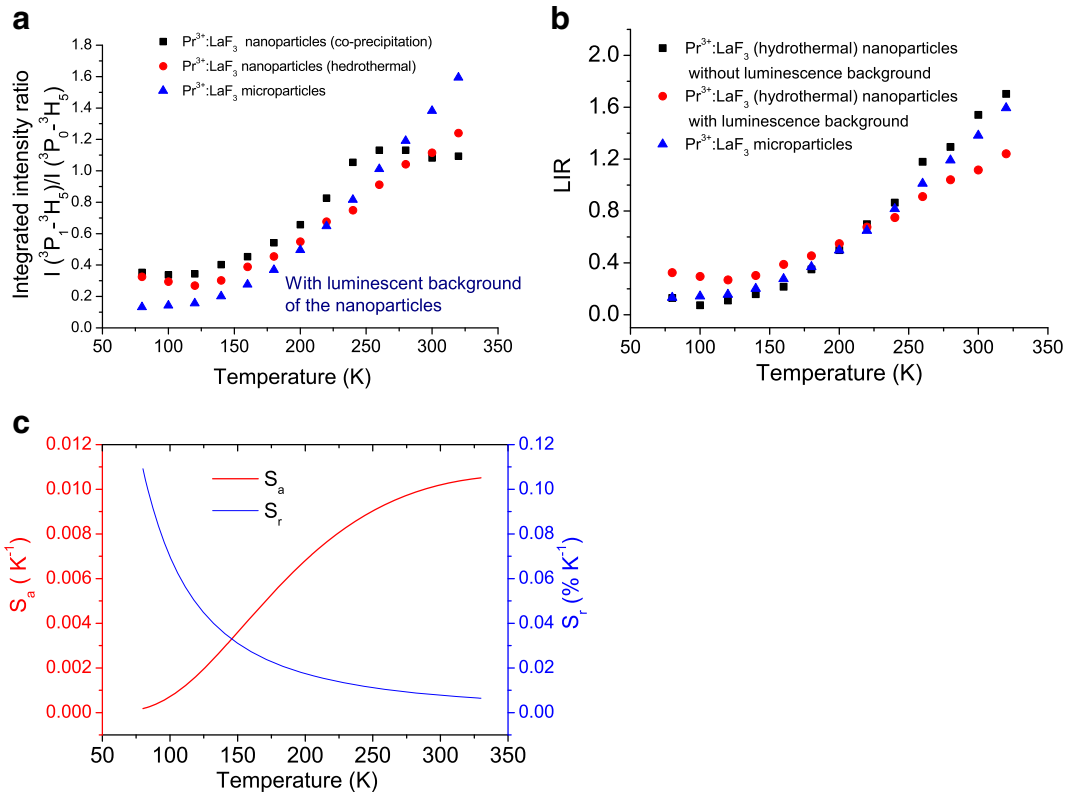

Fig. 9 **a** Integrated intensity ratio of the Pr^{3+}:LaF_3 nanoparticles synthesized via co-precipitation method, Pr^{3+}:LaF_3 nanoparticles synthesized via hydrothermal method, and the Pr^{3+}:LaF_3 microparticles (c) as a function of temperature. **b** Integrated intensity ratio of the Pr^{3+}:LaF_3 (hydrothermal) before and after removing of the luminescence background, Pr^{3+}:LaF_3 microparticles as a function of temperature. **c** Absolute and relative temperature sensitivity curves of Pr^{3+}:LaF_3 and Pr^{3+}:$LiYF_4$ microparticles

present work is notable. This fact can be explained by the bands overlap between $^3P_1 \rightarrow {}^3H_5$ and $^3P_0 \rightarrow {}^3H_5$ emissions. Indeed, in work (Cao et al. 2014) LIR between the overlapping $^4I_{15/2} \rightarrow {}^6H_{15/2}$ (455 nm) and $^4F_{9/2} \rightarrow {}^6H_{15/2}$ (478 nm), emission peaks of Dy^{3+} gives rise to $\Delta E = 1046\ cm^{-1}$ between $^4I_{15/2}$ and $^4F_{9/2}$ thermally coupled levels. However, LIR between spectrally separated $^4I_{15/2} \rightarrow {}^6H_{15/2}$ (455 nm) and $^4F_{9/2} \rightarrow {}^6H_{13/2}$ (573 nm) emission peaks gives rise to another value of $\Delta E = 1373\ cm^{-1}$ between the same thermally coupled levels. In the case of Pr^{3+}-doped $LiYF_4$ and LaF_3, the chosen $^3P_1 \rightarrow {}^3H_5$ and $^3P_0 \rightarrow {}^3H_5$ emission peaks seem to show the same tendency. However, these chosen emission peaks demonstrate the best degree of spectral separation among the registered emission peaks.

Although the studied samples demonstrate close valued of S_a, these samples differ between each other by other properties. As it was discussed above, the spectra of both Pr^{3+}:LaF_3 (co-precipitation) and Pr^{3+}:LaF_3 (hydrothermal) nanoparticles demonstrate undesirable luminescence background which hinders their thermometric properties. The utilization of luminescence background removing procedures can be a source of mistakes. Additionally, this removing procedure significantly complicates the signal

Table 4 The values of S_a and ΔE for Pr^{3+}:$LiYF_4$ nanoparticles, Pr^{3+}:$LiYF_4$ microparticles, and Pr^{3+}:LaF_3 microparticles

Sample	S_a (K^{-1}) at 300 K	S_r ($\%K^{-1}$) $*10^{-4}$ at 300 K	ΔE (cm^{-1}) determined here	ΔE (cm^{-1}) theoretical
Pr^{3+}:$LiYF_4$ nanoparticles	0.0117 ± 0.0010	6.4 ± 0.2	480 ± 4	556
Pr^{3+}:$LiYF_4$ microparticles	0.0106 ± 0.0010	6.6 ± 0.2	486 ± 4	556
Pr^{3+}:LaF_3 microparticles	0.0102 ± 0.0012	6.6 ± 0.2	507 ± 6	587

processing procedure. Hence, the use of Pr^{3+}:LaF_3 luminescent nanothermometers seems to be effective only for microsized particles. The same tendency is observed in (Zhou et al. 2014). The Pr^{3+}:$NaYF_4$ microparticles demonstrate good performance, in turn, Pr^{3+}:$NaYF_4$ nanoparticles show the undesirable luminescent background. The presence of the luminescence background limits the use of Pr^{3+}:LaF_3 luminescent nanothermometers in some specific areas such as biology and medicine. Unlike, the spectra of both Pr^{3+}:$LiYF_4$ nanoparticles and microparticles do not demonstrate the luminescence background. In turn, the ability to obtain both nanosized and microsized particles expands the fields of application.

Conclusions

In the present work, we make a comparison of Pr^{3+}:LaF_3 and Pr^{3+}:$LiYF_4$ luminescent nano- and microthermometer performances. We studied Pr^{3+}:LaF_3 (co-precipitation), Pr^{3+}:LaF_3 (hydrothermal), and Pr^{3+}:LaF_3 microparticles as well as Pr^{3+}:$LiYF_4$ nanoparticles and Pr^{3+}:LaF_3 microparticles. According to the X-ray diffraction, Pr^{3+}:LaF_3 (co-precipitation) and Pr^{3+}:LaF_3 (hydrothermal) nanoparticles are hexagonal-structured nanocrystals. Pr^{3+}:$LiYF_4$ nanoparticles are tetragonal-structured nanocrystals. The average diameters of Pr^{3+}:LaF_3 (co-precipitation), Pr^{3+}:LaF_3 (hydrothermal), and Pr^{3+}:$LiYF_4$ nanoparticles are 13.9, 19.4, and 33.3 nm, respectively. The Pr^{3+}:LaF_3 (co-precipitation) and Pr^{3+}:LaF_3 (hydrothermal) nanoparticles demonstrate broadband luminescence caused by crystal lattice defects (luminescence background). In the case of Pr^{3+}:LaF_3 (co-precipitation) nanoparticles, luminescence background is more pronounced. This luminescence background notably decreases the temperature sensitivity of these samples especially for Pr^{3+}:LaF_3 (co-precipitation) nanoparticles. The luminescent background removing procedure significantly complicates the signal processing procedure. Pr^{3+}:LaF_3 microparticles, Pr^{3+}:$LiYF_4$ nanoparticles, and Pr^{3+}:LaF_3 microparticles do not demonstrate the luminescence background. The absolute temperature sensitivity S_a of Pr^{3+}:$LiYF_4$ nanoparticles, Pr^{3+}:$LiYF_4$ microparticles, and Pr^{3+}:LaF_3 microparticles at 300 K are 0.0117 ± 0.0010, 0.0106 ± 0.0010, and 0.0102 ± 0.0012 K^{-1}, respectively. Although the values of S_a are very close for these samples, the nanosized dimensionality of Pr^{3+}:$LiYF_4$ nanoparticles allows achieving high spatial resolution and expanding the fields of application of Pr^{3+}:$LiYF_4$ nanoparticles.

Acknowledgments The synthesis, XRD experiments, and TEM microscopy experiments were funded by the subsidy allocated to Kazan Federal University for the state assignment in the sphere of scientific activities [3.1156.2017/4.6] and [3.5835.2017/6.7]. The optical spectroscopy experiments were funded by the research grant of Kazan Federal University. Microscopy studies were carried out at the Interdisciplinary Center for Analytical Microscopy of Kazan Federal University.

Compliance with ethical standards

Conflict of interest The authors declare that they have no conflict of interest.

References

Alakshin EM, Blokhin DS, Sabitova AM, Klochkov AV, Klochkov VV, Kono K (2012) Experimental proof of the existence of water clusters in fullerene-like PrF_3 nanoparticles. JETP Lett 96(3):181–183

Becerro AI, Gonzalez-Mancebo D, Ocaña M (2015) Uniform, luminescent Eu:LuF_3 nanoparticles. J Nanopart Res 17(1):58

Bednarkiewicz A, Stefanski M, Tomala R, Hreniak D, Strek W (2015) Near infrared absorbing near infrared emitting highly-sensitive luminescent nanothermometer based on Nd3+ to Yb3+ energy transfer. Phys Chem Chem Phys 17(37): 24315–24321

Brites CDS, Millán A, Carlos LD (2016) Lanthanides in luminescent thermometry. In: Handbook on the Physics and Chemistry of Rare Earths, vol 49. Elsevier, Amsterdam, pp 339–427

Brites CD, Balabhadra S, Carlos LD (2019) Lanthanide-based thermometers: at the cutting-edge of luminescence thermometry. Adv Opt Mater 7(5):1801239. https://doi.org/10.1002/adom.201801239

Bu YY, Cheng SJ, Wang XF, Yan XH (2015) Optical thermometry based on luminescence behavior of Dy^{3+}-doped transparent LaF_3 glass ceramics. Appl Phys A 121(3):1171–1178

Cao Z, Zhou S, Jiang G, Chen Y, Duan C, Yin M (2014) Temperature dependent luminescence of Dy^{3+} doped $BaYF_5$ nanoparticles for optical thermometry. Curr Appl Phys 14(8):1067–1071

Carnall WT, Fields PR, Sarup R (1969) $^1S_0$ Level of Pr^{3+} in crystal matrices and energy-level parameters for the $^4f_2$ configuration of Pr^{3+} in LaF_3. J Chem Phys 51(6):2587–2591

Clement S, Deng W, Drozdowicz-Tomsia K, Liu D, Zachreson C, Goldys EM (2015) Bright, water-soluble CeF_3 photo-, cathodo-, and X-ray luminescent nanoparticles. J Nanopart Res 17(1):7

Davies GL, O'Brien J, Gun'ko YK (2017) Rare earth doped silica nanoparticles via thermolysis of a single source metallasilsesquioxane precursor. Sci Rep 7:45862

Dong B, Hua RN, Cao BS, Li ZP, He YY, Zhang ZY, Wolfbeis OS (2014) Size dependence of the upconverted luminescence of

$NaYF_4$:Er,Yb microspheres for use in ratiometric thermometry. Phys Chem Chem Phys 16(37):20009–20012

Esterowitz L, Bartoli FJ, Allen RE, Wortman DE, Morrison CA, Leavitt RP (1979) Energy levels and line intensities of Pr^{3+} in $LiYF_4$. Phys Rev B 19(12):6442

Fedorov PP, Luginina AA, Kuznetsov SV, Osiko VV (2011) Nanofluorides. J Fluor Chem 132(12):1012–1039

Feng W, Sun LD, Zhang YW, Yan CH (2010) Synthesis and assembly of rare earth nanostructures directed by the principle of coordination chemistry in solution-based process. Coord Chem Rev 254(9-10):1038–1053

Fu L, Fu Z, Yu Y, Wu Z, Jeong JH (2015) An Eu/Tb-codoped inorganic apatite $Ca_5(PO_4)_3F$ luminescent thermometer. Ceram Int 41(5):7010–7016

Geitenbeek RG, Vollenbroek JC, Weijgertze HM, Tregouet CB, Nieuwelink AE, Kennedy CL, Weckhuysen BM, Lohse D, van Blaaderen A, van den Berg A, Odijk M, Meijerink A (2019) Luminescence thermometry for in situ temperature measurements in microfluidic devices. Lab Chip 19(7): 1236–1246

Gharouel S, Labrador-Páez L, Haro-González P, Horchani-Naifer K, Férid M (2018) Fluorescence intensity ratio and lifetime thermometry of praseodymium phosphates for temperature sensing. Journal of Luminescence. 201:372–383.

Gharouel S, Marciniak L, Lukowiak A, Strek W, Horchani-Naifer K, Férid M (2019) The impact of grain size, Pr^{3+} concentration, and host composition on the non-contact temperature sensing abilities of polyphosphate nano-and microcrystals. J Rare Earths 37(8):812–818. https://doi.org/10.1016/j.jre.2018.12.001

Guozhong C (2004) Nanostructures and nanomaterials: synthesis, properties and applications. World scientific, Singapore

Jaque D, Vetrone F (2012) Luminescence nanothermometry. Nanoscale 4(15):4301–4326

Jia LP, Yan B, Zhang Q (2013) Barium rare earth fluoride nanocrystals: high temperature solution synthesis, characterization and luminescence. J Nanopart Res 15(4):1540

Khiari S, Velázquez M, Moncorgé R, Doualan JL, Camy P, Ferrier A, Diaf M (2008) Red-luminescence analysis of Pr^{3+} doped fluoride crystals. J Alloys Compd 451(1-2):128–131

Kim SY, Won YH, Jang HS (2015) A strategy to enhance Eu^{3+} emission from $LiYF_4$:Eu nanophosphors and green-to-orange multicolor tunable, transparent nanophosphor-polymer composites. Sci Rep 5:7866

Kuznetsov SV, Morozov OA, Gorieva VG, Mayakova MN, Marisov MA, Voronov VV (2018) Synthesis and luminescence studies of CaF_2:Yb:Pr solid solutions powders for photonics. J Fluor Chem 211:70–75

Li C, Lin J (2010) Rare earth fluoride nano-/microcrystals: synthesis, surface modification and application. J Mater Chem 20(33):6831–6847

Liu H, Lu W, Wang H, Rao L, Yi Z, Zeng S, Hao J (2013) Simultaneous synthesis and amine-functionalization of single-phase $BaYF_5$: Yb/Er nanoprobe for dual-modal in vivo upconversion fluorescence and long-lasting X-ray computed tomography imaging. Nanoscale 5(13):6023–6029

Liu J, Van Deun R, Kaczmarek AM (2019) Eu^{3+}, Tb^{3+}-and Er^{3+}, Yb^{3+}-doped α-MoO_3 nanosheets for optical luminescent thermometry. Nanomaterials 9(4):646. https://doi.org/10.3390/nano9040646

Lyapin AA, Gorieva VG, Korableva SL, Artemov SA, Ryabochkina PA, Semashko VV (2016) Diode-pumped $LiY_{0.3}Lu_{0.7}F_4$:Pr and $LiYF_4$:Pr red lasers. Laser Phys Lett 13(12):125801

Ma L, Chen WX, Zheng YF, Zhao J, Xu Z (2007) Microwave-assisted hydrothermal synthesis and characterizations of PrF_3 hollow nanoparticles. Mater Lett 61(13):2765–2768

Mahalingam V, Vetrone F, Naccache R, Speghini A, Capobianco JA (2009) Colloidal Tm^{3+}/Yb^{3+}-doped $LiYF_4$ nanocrystals: multiple luminescence spanning the UV to NIR regions via low-energy excitation. Adv Mater 21(40):4025–4028. https://doi.org/10.1002/adma.200901174

Müller S, Calmano T, Metz P, Hansen NO, Kränkel C, Huber G (2012) Femtosecond-laser-written diode-pumped Pr:$LiYF_4$ waveguide laser. Opt Lett 37(24):5223–5225

Nizamutdinov AS, Semashko VV, Naumov AK, Korableva SL, Abdulsabirov RY, Polivin AN, Marisov MA (2007) Optical and gain properties of series of crystals $LiF–YF_3–LuF_3$ doped with Ce^{3+} and Yb^{3+} ions. J Lumin 127(1):71–75

Pan Z, James K, Cui Y, Burger A, Cherepy N, Payne SA, Morgan SH (2008) Terbium-activated lithium–lanthanum–aluminosilicate oxyfluoride scintillating glass and glass-ceramic. Nucl Instrum Methods Phys Res Sect A 594(2):215–219

Piñol R, Brites CD, Silva NJ, Carlos LD, Millán A (2019) Nanoscale thermometry for hyperthermia applications. Nanomaterials for Magnetic and Optical Hyperthermia Applications. Elsevier, Amsterdam, pp 139–172

Pudovkin MS, Rakhmatullin RM (2020) Fluoride nanoparticles for biomedical applications. In: Nanoparticles in Medicine. Springer, Singapore, pp 135–174. https://doi.org/10.1007/978-981-13-8954-2_5

Pudovkin MS, Zelenikhin PV, Krasheninnikova AO, Korableva SL, Nizamutdinov AS, Alakshin EM et al (2016) Photo-induced toxicity of PrF_3 and LaF_3 nanoparticles. Opt Spectrosc 121(4):538–543

Pudovkin MS, Morozov OA, Pavlov VV, Korableva SL, Lukinova EV, Osin YN et al (2017) Physical background for luminescence thermometry sensors based on Pr^{3+}. J Nanomater 2017:3108586

Pudovkin MS, Zelenikhin PV, Shtyreva V, Morozov OA, Koryakovtseva DA, Pavlov VV et al (2018) Co-precipitation method of synthesis, characterization, and cytotoxicity of Pr^{3+}: LaF_3 (C_{Pr} = 3, 7, 12, 20, 30%) nanoparticles. J Nanotechnol 2018:8516498

Pudovkin MS, Koryakovtseva DA, Lukinova EV, Korableva SL, Khusnutdinova RS, Kiiamov AG et al (2019a) Characterization of Pr-doped LaF_3 nanoparticles synthesized by different variations of co-precipitation method. J Nanomater 2019:549325. https://doi.org/10.1155/2019/7549325

Pudovkin MS, Koryakovtseva DA, Lukinova EV, Korableva SL, Khusnutdinova RS, Kiiamov AG et al (2019b) Luminescence nanothermometry based on Pr3+:LaF3 single core and Pr3+:LaF3/LaF3 core/shell nanoparticles. Adv Mater Sci Eng 2019:2618307. https://doi.org/10.1155/2019/2618307

Rahman P, Green M (2009) The synthesis of rare earth fluoride based nanoparticles. Nanoscale 1(2):214–224

Rakhmatullin RM, Pudovkin MS, Semashko VV (2019) EPR evidence of surface paramagnetic defects formation due to

annealing of LaF_3 nanoparticles. Magn Reson Solids Electron J 21(4)

Rao CNR, Müller A, Cheetham AK (eds) (2006) The chemistry of nanomaterials: synthesis, properties and applications. John Wiley & Sons

Runowski M, Stopikowska N, Szeremeta D, Goderski S, Skwierczyńska M, Lis S (2019a) Up-converting lanthanide fluoride core@ shell nanorods for luminescent thermometry in the first and second biological windows-β-NaYF4:Yb^{3+}, Er^{3+}@SiO_2 temperature sensor. ACS Appl Mater Interfaces 11(14):13389–13396. https://doi.org/10.1021/acsami.9b00445

Runowski M, Woźny P, Martín IR, Lavín V, Lis S (2019b) Praseodymium doped YF_3:Pr^{3+} nanoparticles as optical thermometer based on luminescence intensity ratio (LIR)–Studies in visible and NIR range. J Lumin 116571

Savchuk OA, Carvajal JJ, Cascales C, Massons J, Aguilo M, Diaz F (2016) Thermochromic upconversion nanoparticles for visual temperature sensors with high thermal, spatial and temporal resolution. J Mater Chem C 4(27):6602–6613

Scherrer P (1918) Bestimmung der Grösse und der inneren Struktur von Kolloidteilchen mittels Röntgenstrahlen. Nachr Ges Wiss Göttingen 26:98–100

Semashko VV, Pudovkin MS, Cefalas AC, Zelenikhin PV, Gavriil VE, Nizamutdinov AS, Kollia Z, Ferraro A, Sarantopoulou E (2018) Tiny rare-earth fluoride nanoparticles activate tumour cell growth via electrical polar interactions. Nanoscale Res Lett 13(1):370

Shavelev AA, Nizamutdinov AS, Semashko VV, Korableva SL, Gorieva VG (2014) Distribution coefficient of Pr^{3+} ions in crystals of solid solutions LiF-LuF_3-YF_3-PrF_3. J Phys Conf Ser 560(1):012019. https://doi.org/10.1088/1742-6596/560/1/012019

Vanetsev A, Kaldvee K, Puust L, Keevend K, Nefedova A, Fedorenko S (2017) Relation of crystallinity and fluorescent properties of LaF_3:Nd^{3+} nanoparticles synthesized with different water-based techniques. Chem Sel 2:4874–4881. https://doi.org/10.1002/slct.201701075

Wang X, Li Y (2003) Fullerene-like rare-earth nanoparticles. Angew Chem Int Ed 42:3497–3500. https://doi.org/10.1002/anie.200351006

Wang J, Wang F, Xu J, Wang Y, Liu Y, Chen X, Liu X (2010) Lanthanide-doped $LiYF_4$ nanoparticles: Synthesis and multicolor upconversion tuning. C R Chim 13(6-7):731–736

Yang JM, Yang H, Lin L (2011) Quantum dot nanothermometers reveal heterogeneous local thermogenesis in living cells. ACS Nano 5(6):5067–5071

Ye S, Hu R, Jiang N, Wang H, Wang D (2015) pH value manipulated phase transition, microstructure evolution and tunable upconversion luminescence in Yb^{3+}/Er^{3+} codoped $LiYF_4$/YF_3 nanoparticles. Dalton Trans 44(35):15583–15590. https://doi.org/10.1039/C5DT01552A

Yu Q, Rodriguez EM, Naccache R, Forgione P, Lamoureux G, Sanz-Rodriguez F (2014) Chemical modification of temoporfin–a second generation photosensitizer activated using upconverting nanoparticles for singlet oxygen generation. Chem Commun 50(81):12150–12153

Zhou S, Jiang G, Wei X, Duan C, Chen Y, Yin M (2014) Pr^{3+}-Doped β-$NaYF_4$ for temperature sensing with fluorescence intensity ratio technique. J Nanosci Nanotechnol 14(5):3739–3742